NRL Report 7005

A Study of Sea Return at Normal and Near-Normal Incidence

O. D. SLEDGE AND S. F. GEORGE

Radar Analysis Staff
Radar Division

January 30, 1970

NAVAL RESEARCH LABORATORY
Washington, D.C.

Security Classification

DOCUMENT CONTROL DATA - R & D

(Security classification of title, body of abstract and indexing annotation must be entered when the overall report is classified)

1. ORIGINATING ACTIVITY (Corporate author)	2a. REPORT SECURITY CLASSIFICATION
Naval Research Laboratory Washington, D.C. 20390	Unclassified 2b. GROUP

3. REPORT TITLE

A STUDY OF SEA RETURN AT NORMAL AND NEAR-NORMAL INCIDENCE

4. DESCRIPTIVE NOTES (Type of report and inclusive dates)

A final report on one phase of the problem.

5. AUTHOR(S) (First name, middle initial, last name)

O.D. Sledge and S.F. George

6. REPORT DATE	7a. TOTAL NO. OF PAGES	7b. NO. OF REFS
January 30, 1970	23	11

8a. CONTRACT OR GRANT NO.	9a. ORIGINATOR'S REPORT NUMBER(S)
NRL Problem R02-54 b. PROJECT NO. RF 05-151-402-4010 c. d.	NRL Report 7005 9b. OTHER REPORT NO(S) (Any other numbers that may be assigned this report)

10. DISTRIBUTION STATEMENT

This document has been approved for public release and sale; its distribution is unlimited.

11. SUPPLEMENTARY NOTES	12. SPONSORING MILITARY ACTIVITY
	Department of the Navy (Office of Naval Research), Washington, D.C. 20360

13. ABSTRACT

Recently, interest has been manifested in using the sea return observed by an airborne radar as a possible continuous monitor of the condition of the sea surface. As a step in analytically evaluating the concept, a brief study is presented of the sea return as seen by a radar viewing the sea at near-normal incidence.

Part I contains a theoretical treatment based on the work of Kodis and Barrick. Neglecting multiple scattering effects and assuming that the radius of curvature of the surface as well as the rms roughness height of the surface are both larger than three radar wavelengths, Kodis showed that the scattering cross section of the rough surface consists of the linear sum of the scattering cross sections of the individual specular points lying in the illuminated area of the surface. Using the specular point model of Kodis, Barrick derived an expression for the backscattering cross section per unit area of a rough surface with a Gaussian slope distribution. Barrick's expression for σ^0 involves the mean square slope of the random surface, the angle of incidence of the plane wave of illumination, and the Fresnel reflection coefficient of the surface for normal incidence.

The formula of Barrick, derived for a plane wave, also applies to the case of a narrow-beam radar above the sea, provided that certain restrictions on the magnitudes of angle of incidence of the radar beam, the beamwidth, and the mean square slope of the sea surface hold. Using Barrick's formula for σ^0 and data from Cox and Munk relating the mean square slope of the sea to wind speed, curves are drawn showing σ^0 as a function of wind velocity near normal incidence and σ^0 vs angle of incidence for various sea conditions. Contours are

(OVER)

14. KEY WORDS	LINK A		LINK B		LINK C	
	ROLE	WT	ROLE	WT	ROLE	WT
Sea clutter near normal incidence Sea return by satellite radar Sea surface monitor Specular point clutter model Schooley facet model Radar sea return Radar backscatter						

also plotted for σ^0 values 3, 6, and 10 dB down from maximum for radar angle of incidence vs wind velocity.

Part II applies the statistics of the Schooley measurements to the same problem of calculating σ^0. The Schooley data take the form of two distributions: (a) the probability density of facet inclination angles and (b) the distribution of average facet length vs facet inclination angles and wind velocity. Using these data and assuming a facet model based on diffraction theory, calculations are made of σ^0 for radars at λ = 1, 3, and 10 cm vs wind velocity. These curves show a remarkable similarity to those of Part I despite the rather disparate models. Curves are also shown of the same nature as in Part I for λ = 3 cm only; however, there is a difference in the results between radars looking upwind and downwind. This comes from the Schooley data which comprise a one-dimensional cut along the direction of the wind. The facet model also shows a frequency dependence arising from the diffraction effects.

The two sea models examined in this report do not agree in quantitative detail, but there are many striking similarities considering the very different models. Further experimental measurements at normal and near-normal incidence would be required to confirm the theoretical values of the deviation of the angle of incidence of the radar beam off vertical necessary to reduce σ^0 in level by 3, 6, or 10 dB for various sea conditions.

CONTENTS

Abstract	ii
Problem Status	iii
Authorization	iii
INTRODUCTION	1
PART I — THEORETICAL STUDY OF σ^0 NEAR NORMAL INCIDENCE	1
Background	1
Theoretical Model	2
Calculated Results	6
PART II — STUDY OF σ^0 NEAR NORMAL INCIDENCE USING SCHOOLEY FACET MODEL	10
Background	10
Calculations of σ^0 at Normal Incidence	10
Calculations of σ^0 Near Normal Incidence	12
A COMPARISON OF THE SPECULAR POINT AND SCHOOLEY FACET MODELS	14
CONCLUSIONS	16
REFERENCES	17
APPENDIX — A More General Expression for σ^0 at Normal Incidence	18

ABSTRACT

Recently, interest has been manifested in using the sea return observed by an airborne radar as a possible continuous monitor of the condition of the sea surface. As a step in analytically evaluating the concept, a brief study is presented of the sea return as seen by a radar viewing the sea at near-normal incidence.

Part I contains a theoretical treatment based on the work of Kodis and Barrick. Neglecting multiple scattering effects and assuming that the radius of curvature of the surface as well as the rms roughness height of the surface are both larger than three radar wavelengths, Kodis showed that the scattering cross section of the rough surface consists of the linear sum of the scattering cross sections of the individual specular points lying in the illuminated area of the surface. Using the specular point model of Kodis, Barrick derived an expression for the backscattering cross section per unit area of a rough surface with a Gaussian slope distribution. Barrick's expression for σ^0 involves the mean square slope of the random surface, the angle of incidence of the plane wave of illumination, and the Fresnel reflection coefficient of the surface for normal incidence.

The formula of Barrick, derived for a plane wave, also applies to the case of a narrow-beam radar above the sea, provided that certain restrictions on the magnitudes of angle of incidence of the radar beam, the beamwidth, and the mean square slope of the sea surface hold. Using Barrick's formula for σ^0 and data from Cox and Munk relating the mean square slope of the sea to wind speed, curves are drawn showing σ^0 as a function of wind velocity near normal incidence and σ^0 vs angle of incidence for various sea conditions. Contours are also plotted for σ^0 values 3, 6, and 10 dB down from maximum for radar angle of incidence vs wind velocity.

Part II applies the statistics of the Schooley measurements to the same problem of calculating σ^0. The Schooley data take the form of two distributions: (a) the probability density of facet inclination angles and (b) the distribution of average facet length vs facet inclination angles and wind velocity. Using these data and assuming a facet model based on diffraction theory, calculations are made of σ^0 for radars at λ = 1, 3, and 10 cm vs wind velocity. These curves show a remarkable similarity to those of Part I despite the rather disparate models. Curves are also shown of the same nature as in Part I for λ = 3 cm only; however, there is a difference in the results between radars looking upwind and downwind. This comes from the Schooley data which comprise a one-dimensional cut along the direction of the wind. The facet model also shows a frequency dependence arising from the diffraction effects.

The two sea models examined in this report do not agree in quantitative detail, but there are many striking similarities considering the very different models. Further experimental measurements at normal and near-normal

incidence would be required to confirm the theoretical values of the deviation of the angle of incidence of the radar beam off vertical necessary to reduce σ^0 in level by 3, 6, or 10 dB for various sea conditions.

PROBLEM STATUS

This is a final report on one phase of the problem.

AUTHORIZATION

NRL Problem R02-54
Project RF 05-151-402-4010

Manuscript submitted October 15, 1969.

A STUDY OF SEA RETURN AT NORMAL AND NEAR-NORMAL INCIDENCE

INTRODUCTION

This report is divided into two parts. Part I contains a theoretical study of the sea return that could be expected from an airborne radar looking at the sea at normal and near-normal incidence. Part II contains the results of applying the Schooley (1) facet model and his measurements of clutter to the same problem.

PART I—THEORETICAL STUDY OF σ^0 NEAR NORMAL INCIDENCE

Background

In a recent paper, Kodis (2) treats the problem of electromagnetic scattering from a rough surface. Beginning with an exact integral equation for the far-field scatter, Kodis' derivation differs from the approaches used by others (3-6) in that the physical optics integral is evaluated (by the method of stationary phase) before averaging over an ensemble of surfaces instead of afterwards. This approach sheds light on the physical mechanism responsible for the scattered field. In particular, Kodis' result shows that to the first approximation the average backscattering cross section per unit area of a perfectly conducting rough surface is

$$\sigma^0 = \pi \langle N \rangle \langle | r_1 r_2 | \rangle , \tag{1}$$

where $\langle N \rangle$ is the average number of specular points per unit area of the surface, and $\langle | r_1 r_2 | \rangle$ equals the average absolute value of the product of the principal radii of curvature at the illuminated specular points.

The validity of Eq. (1) is subject to the following restrictions:

1. The radius of curvature of the surface is everywhere greater than three wavelengths of the incident radiation. This condition implies that diffraction effects may be neglected.

2. Multiple scattering between various parts of the surface is neglected.

3. The rms roughness height of the surface exceeds three wavelengths of the incident radiation. This condition allows one to sum linearly the scattering cross sections of the individual specular points lying in the illuminated area of the surface to form the radar cross section of the illuminated area without regard to the phase relations between the backscattered fields of the specular points. However, this restriction prohibits the consideration of capillaries as reflectors.

In Kodis' theoretical model the rough, perfectly conducting surface was illuminated by a plane electromagnetic wave incident in free space above the scattering surface, the mean plane of which was horizontal.

Equation (1) has a few interesting features. In the first place, it shows that the radar cross section of a specular point is equal to the geometric-optics cross section of a sphere whose radius is the geometrical mean of the principal radii of curvature at the specular points. Secondly, the dependence on the angle of incidence is implicit in $\langle N \rangle$, since $\langle | r_1 \; r_2 | \rangle$ is probably not a very sensitive function of this angle. It seems clear that the number of specular points is near a maximum at normal incidence and decreases as the angle of incidence increases.

To carry out backscattering calculation with Eq. (1), the statistics of the surface must be specified and a study made of how these are related to the average number of illuminated specular points per unit area and $\langle | r_1 \; r_2 | \rangle$ at the specular points. Recently, Barrick (7) performed this operation for a random, finitely conducting surface with a Gaussian distribution of surface height. Barrick finds that the radar cross section per unit area of the Gaussian surface, based on Eq. (1), is

$$\sigma^0 = \frac{\sec^4 \theta_i}{\overline{S^2}} \exp \left(- \tan^2 \theta_i / \overline{S^2} \right) | R_s \; (0) |^2 \tag{2}$$

where $R_s \; (0)$ is the Fresnel reflection coefficient of the space-to-surface interface for normal incidence, $\overline{S^2}$ is the mean square slope of the rough surface, and θ_i is the angle of incidence of the illuminating uniform plane wave measured with respect to the normal to the mean plane of the random surface. Although Barrick makes a statistical approximation in his derivation leading to Eq. (2) which is difficult to justify, his result is in agreement with the work of others, in particular Hagfors (4).

The purpose of Part I of this report is to investigate the radar cross section per unit area of the sea surface as viewed by an airborne, narrow-beam radar using the theories of Kodis and Barrick cited above.

Theoretical Model

Figure 1 shows the narrow-beam radar lying in the yz plane above the sea, the mean plane of which is the xy plane. It is assumed that the roughness height of the sea surface has a Gaussian distribution. Further, we assume that restrictions 1, 2, and 3

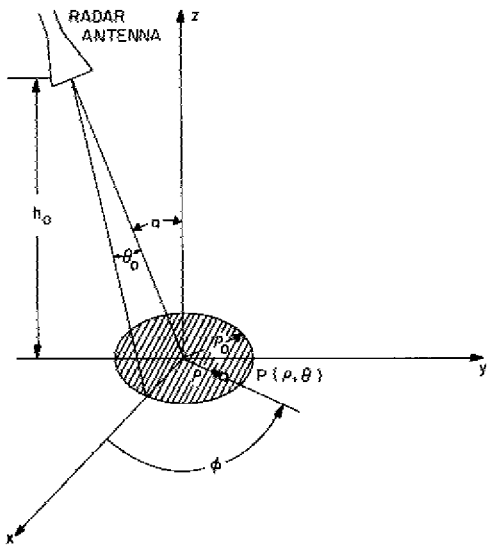

Fig. 1 - Geometry of the problem

placed on the model of Kodis hold. It follows from Eq. (2) that the radar cross section of the illuminated area of the sea surface whose projection on the mean plane is the cross-hatched circular area of Fig. 1 can be expressed approximately in the form of the following surface integral:

$$\sigma_s = |R_s(0)|^2 \int_0^{\rho_0} \int_0^{2\pi} \frac{\sec^4\gamma}{\overline{S^2}} \exp\left(-\tan^2\gamma/\overline{S^2}\right) d\phi\, \rho\, d\rho, \tag{3}$$

where

$\rho_0 = h_0 \sec\alpha \tan\theta_0$ = radius of circular projected illuminated area

h_0 = height of radar above the sea

α = angle of incidence of radar beam

γ = local angle of incidence to the mean plane of the sea surface at $P(\rho, \phi)$ in the mean plane.

The angle θ_0 corresponds to the 0.1-power point on the major lobe of the axially symmetrical radiation pattern of the radar antenna.

It is easily shown from Fig. 1 that

$$\tan^2\gamma = (\rho/h_0)^2 + \tan^2\alpha + 2(\rho/h_0)\tan\alpha \sin\phi. \tag{4}$$

Upon introducing Eq. (4), Eq. (3) can be written in the form

$$\sigma_s = \frac{h_0^2}{\overline{S^2}} |R_s(0)|^2 \sec^4\alpha \exp\left(-\tan^2\alpha/\overline{S^2}\right) \int_0^{u_0} u \exp\left[-u^2/\overline{S^2}\right] \ell_1\, du$$

$$\sigma^0 = \frac{\sigma_s \langle|\cos\beta|\rangle}{\pi h_0^2 \sec^2\alpha \tan^2\theta_0} \tag{5}$$

$$= \frac{\langle|\cos\beta|\rangle |R_s(0)|^2}{\overline{S^2}\,\pi \tan^2\theta_0} \sec^2\alpha \exp\left(-\tan^2\alpha/\overline{S^2}\right) \int_0^{u_0} u \exp\left(-u^2/\overline{S^2}\right) \ell_1\, du,$$

where

$$\ell_1 = \int_0^{2\pi} \left[C_0^2 + 2C_0 C_1 \sin\phi + C_1^2 \sin^2\phi\right] \exp\left[-\frac{2(\rho/h_0)}{\overline{S^2}} \tan\alpha \sin\phi\right] d\phi$$

$$C_0 = 1 + (\rho/h_0)^2/\sec^2\alpha \tag{6}$$

$$u = \rho/h_0$$

$$u_0 = \rho_0/h_0$$

$$C_1 = 2(\rho/h_0)\tan\alpha/\sec^2\alpha$$

Using the Fourier series representation,

$$\exp(x\cos\beta) = I_0(x) + 2\sum_{n=1}^{\infty} I_n(x)\cos n\beta, \tag{7}$$

where $I_n(x)$ is the nth-order, modified Bessel function of the first kind. Letting $\phi = \beta - (\pi/2)$, the definite integral ℓ_1 becomes

$$\ell_1 = 2\pi\left[(C_0^2 + C_1^2/2)\, I_0(x) - 2C_0C_1C_1(x) + C_1^2/2\, I_2(x)\right], \tag{8}$$

where $x = [2(\rho/h_0)\tan\alpha]/\overline{S^2}$. With the recurrence relation

$$I_2(x) = \frac{2}{x} I_1(x) + I_0(x), \tag{9}$$

we can eliminate $I_2(x)$ from Eq. (8), so that our formula for ℓ_1 becomes

$$\ell_1 = 2\pi\left[C_0^2 + C_1^2\ I_0(x) - C_1\{2C_0 + C_1/x\}\, I_1(x)\right] \tag{10}$$

To evaluate the remaining integral in u, we limit $u_0^2/\overline{S^2}$ to values less than 1/10. Under these conditions, we may closely approximate the exponential function appearing in the integrand of Eq. (5) by the first two terms of its power series representation. Using the relation

$$\int_0^x x^n I_{n-1}(x)\, dx = z^n I_n(z) \tag{11}$$

with Eq. (9) and integrating by parts finally results in the following approximate expression for σ_s:

$$\sigma_S = \left[\pi h_0^2 \left|R_S(0)\right|^2 \frac{\sec^6\alpha}{S^2} \exp(-\tan^2\alpha/\overline{S^2})\tan^2\theta_0\right] K, \tag{12}$$

which holds for $u_0^2/\overline{S^2} < 0.1$, where

$$K = (1 + u_0 A)\frac{2m}{u_0} I_1\left(\frac{u_0}{m}\right) - 4m\,(mA + B)\, I_2\left(\frac{u_0}{m}\right) \tag{13}$$

and

$$A = \frac{2}{\sec^2\alpha}(1 + 2\sin^2\alpha) - 1/\overline{S^2}$$

$$B = \frac{\tan\alpha}{\sec^2\alpha}(2 + \overline{S^2}/\sec^2\alpha)$$

$$u_0 = \sec\alpha\tan\theta_0$$

$$m = \frac{\overline{S^2}}{2\tan\alpha}$$

The illuminated area of the sea projected onto the mean plane of the sea* is simply $\pi h_0^2 \sec^2 \alpha \tan^2 \theta_0$; hence, the average radar cross section per unit area of the sea can be approximated by the expression

$$\sigma^0 = \frac{\sigma_S \langle|\cos \beta|\rangle}{\pi h_0^2 \sec^2 \alpha \tan^2 \theta_0}$$

$$\sigma^0 = \langle|\cos \beta|\rangle \frac{K|R_S(0)|^2}{\overline{S^2}} \sec^4 \alpha \exp\left(-\tan^2 \alpha/\overline{S^2}\right) \left[u_0^2/\overline{S^2} < 0.1\right]. \quad (14)$$

The quantity $\langle|\cos \beta|\rangle$ is the average absolute value of the cosine of the angle which the plane tangent to the surface makes with the mean plane of the surface.

A comparison of Eq. (14) with Eq. (2) shows that our formula for σ^0 is simply the Barrick's formula modified by the factor $K \langle|\cos \beta|\rangle$.

If we limit the argument of the modified Bessel functions to values less than unity and approximate the Bessel functions appearing in K by the first two terms of their respective power series representations, the following formula for K results:

$$K = 1 + \tan^2 \theta_0 \left\{ \frac{M}{2\overline{S^2} \cos^2 \alpha} - 2M - \sin^2 \alpha \right.$$

$$\left. - \left(1 + \frac{M \tan^2 \theta_0}{\overline{S^2} \cos^2 \alpha}\right)\left[\frac{1}{2\overline{S^2} \cos^2 \alpha} - 1 - 2 \sin^2 \alpha\right]\right\},$$

where $M = (\tan^2 \alpha)/\overline{S^2}$ and

$$\frac{u_0}{M} < 1,$$

$$\frac{u_0^2}{\overline{S^2}} < 0.1. \quad (15)$$

In Fig. 2 we present $(K - 1)$ plotted vs α for the case where $\overline{S^2} = 0.02$ and $\theta_0 = 0.04$ radian.

To relate to practical radar antennas, we give the following example. For $\overline{S^2}$ greater than 0.02, the radar antenna gain must exceed 37 dB or the half-power beamwidth must be less than 2.6 degrees in order to meet the restriction placed on Eq. (14). These figures assume a typical radar antenna with a pencil beam and a 10-dB tapered illumination. For the assumed antenna, θ_0 turns out to be 0.90 of the half-power beamwidth. To satisfy the additional restriction placed on Eq. (15), the angle of incidence of the radar beam α should be 13 degrees or less.

*In arriving at the illuminated area, the side lobes of the radiation pattern are neglected and the main beam is assumed nearly axially symmetrical.

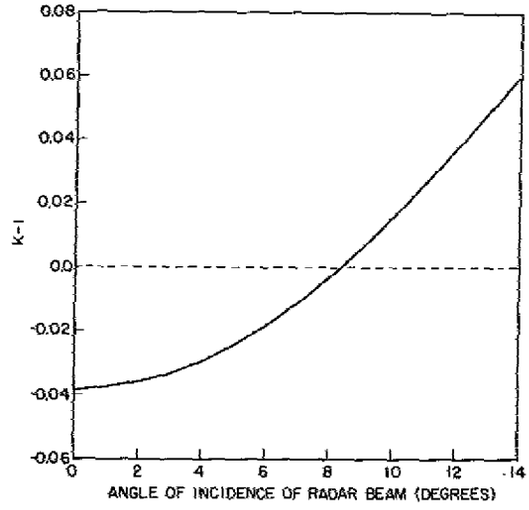

Fig. 2 – A plot of $(K - 1)$ vs angle of incidence for $\overline{S^2} = 0.02$ and $\theta_0 = 0.04$ radian

A study of Eq. (15) reveals that K differs from unity by less than 5 percent, provided

$$\left(\frac{u_0^2}{\overline{S^2}}\right)\left|\frac{\tan^2\alpha}{\overline{S^2}} - 1\right| < 0.10. \tag{16}$$

In the appendix, we consider the limiting case of normal incidence. Starting with Eq. (5), the integral therein is evaluated without the use of approximation. At normal incidence the radar cross section per unit area of the sea becomes

$$\sigma^0 = \frac{\langle|\cos\beta|\rangle|R_S(0)|^2}{\tan^2\theta_0}\left[\left(1 + 2\overline{S^2} + 2\left(\overline{S^2}\right)^2\right)\right.$$

$$\left. - \left(\sec^4\theta_0 + 2\overline{S^2}\sec^2\theta_0 + 2\left(\overline{S^2}\right)^2\right)\exp\left(-\tan^2\theta_0/\overline{S^2}\right)\right]. \tag{17}$$

Unlike Eq. (14), the above expression for σ^0 is not subject to the beamwidth restriction $u_0^2/\overline{S^2} < 0.1$. Equation (17) holds for very calm seas, provided the radiation wavelength is reduced as the sea surface becomes more calm so as to keep the rms roughness height three or more wavelengths.

Calculated Results

In arriving at the calculated results presented in Part I of this report, we shall use Eq. (14) with both $\langle|\cos\beta|\rangle$ and K assigned the value of unity. These approximations introduce only a fraction of a decibel error in σ^0, provided that the wind speed is less than 30 knots and that the restrictions on Eq. (15) and the condition Eq. (16) remain valid. For example, if $\overline{S^2} = 0.02$ and $\tan\theta_0 = 0.017$, the restrictions on Eqs. (15) and (16) hold for any angle of incidence of the radar beam α less than 20 degrees. It is estimated from Schooley's data that $\langle|\cos\beta|\rangle$ is about 0.96 at a 30-knot wind speed. The value used for $|R_S(0)|^2$ in our calculations is 0.65, which is correct for water at radar wavelengths extending from 0.5 to 10 cm.

In Fig. 3 we present a graph showing the relationship between the mean square slope of the sea surface and the wind speed. The linear graph represents the average of many experimental measurements of $\overline{S^2}$ made at optical wavelengths by Cox and Munk (8) who unfortunately did not state the degree to which the sea was developed under the influence of the wind. The wind speed was measured at a point 41 ft above the mean level of the sea. In the remaining figures where wind speed appears, the relationship shown in Fig. 3 is used in its derivation.

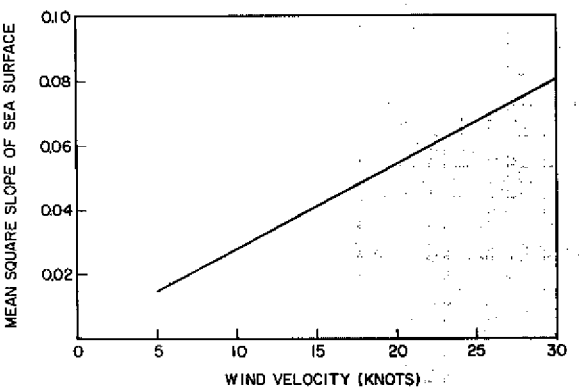

Fig. 3 - The mean square slope of the sea surface as a function of wind velocity (8)

In Fig. 4 we show σ^0 in decibels as a function of wind velocity for various angles of incidence of the radar beam. The small crosses represent data points calculated for an angle of incidence of 2 degrees. It is observed from Fig. 4 that the angle of incidence should be kept to within a tolerance of ±3 degrees of normal for σ^0 to be used as a satisfactory measure of the wind speed.

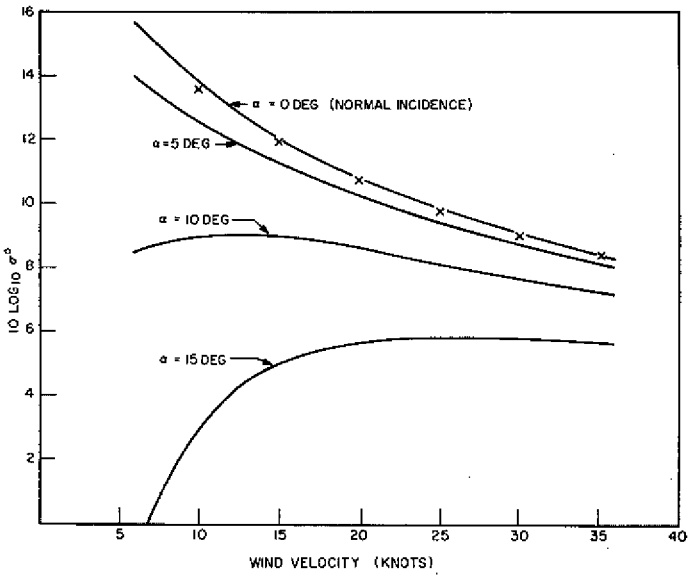

Fig. 4 - The radar cross section per unit area of the sea (in decibels) as a function of wind velocity for angles of incidence of the radar beam of 0, 5, 10, and 15 degrees

In Fig. 5 we present σ^0 in decibels plotted vs the angle of incidence of the radar beam for several constant values of the mean square slope of the sea surface $\overline{S^2}$. A comparison is shown of the theoretical results and the experimental measurements of σ^0 made by Grant and Yaplee (9) at a radar wavelength of 8.6 mm with a half-power beamwidth of 2.4 degrees. The comparison reveals that the graph of Fig. 5 corresponding to a wind speed of 14.6 knots agrees with the results of Grant and Yaplee to within 0.8 dB. At a wind speed of 22.5 knots, the experimental values of σ^0 appear to be 1.2 to 1.8 dB higher than the theoretical values at each angle of beam incidence extending from 0 to 22 degrees. At the lower wind speed of 7 knots, it is found that the level of σ^0 at vertical incidence calculated from the theory of Part I is 1 dB below the experimental value (16 dB). At this lower wind speed, the experimental values of σ^0 decrease much more rapidly with the angle of incidence than the theoretical values of σ^0. The value of σ^0 reaches 0 dB at a beam incidence of 10 degrees in the experimental results, while in the theoretical results this level of σ^0 is not attained until the beam incidence angle becomes 15 degrees. As the wavelength increases, the theoretical and experimental results are separated by wider margins. One reason for this divergence may be that the relationship between $\overline{S^2}$ and wind speed used here was obtained from optical measurements.

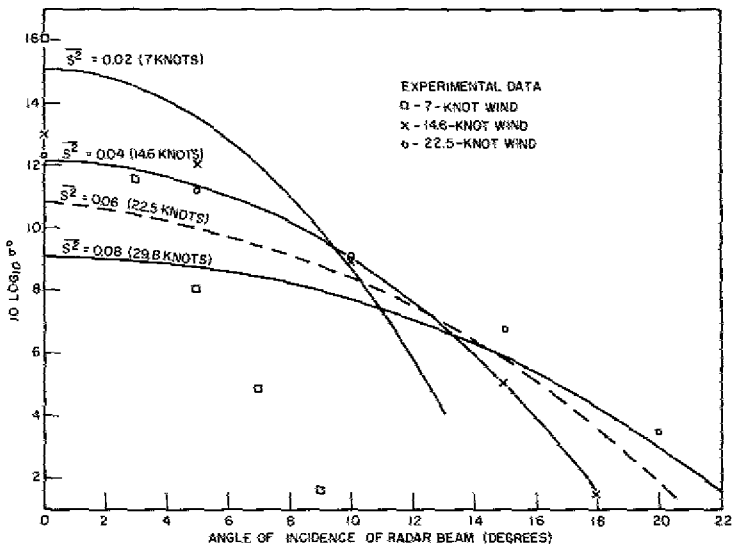

Fig. 5 - The radar cross section per unit area of the sea (in decibels) plotted vs the angle of incidence of the radar beam for several values of $\overline{S^2}$

It is apparent from Fig. 5 that the angle of incidence corresponding to a point 3 dB down from the σ^0 level at normal incidence ($\alpha = 0$) becomes progressively smaller as $\overline{S^2}$ decreases or as the sea becomes calmer. This suggests that one might use the angle of incidence at the -3 dB points as a measure of the roughness of the sea or of the wind velocity. This measure of wind speed or sea roughness has the advantage of being independent of the absolute level of σ^0. From the curves of Fig. 5, we determined the angle of incidence at the points where σ^0 is 3, 6, and 10 dB down relative to the σ^0 level at normal incidence for each value of $\overline{S^2}$. The results appear in the form of the linear graphs shown in Fig. 6, plotted on logarithmic coordinate scales. From the essentially parallel linear graphs of Fig. 6, one can easily show that the graphs can be represented quite well by the following empirical formulas:

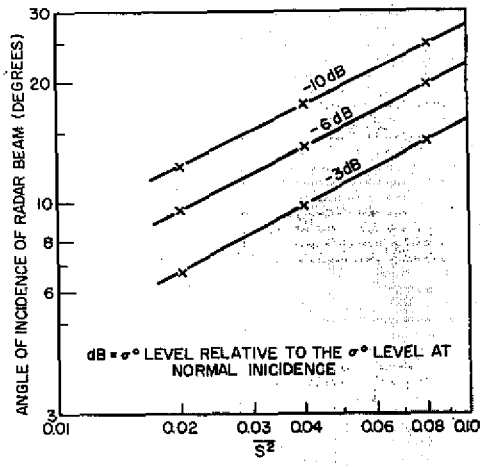

Fig. 6 - The angle of incidence at a given value of $\overline{S^2}$ necessary to maintain σ^0 at a constant level of N dB relative to the σ^0 at normal incidence; N = -3, -6, and -10

$$\alpha_{-3\ dB} = 49 \left(\overline{S^2}\right)^{1/2} \ (degrees) \tag{18}$$

$$\alpha_{-6\ dB} = 68.7 \left(\overline{S^2}\right)^{1/2} \ (degrees) \tag{19}$$

$$\alpha_{-10\ dB} = 87.5 \left(\overline{S^2}\right)^{1/2} \ (degrees) \tag{20}$$

In Fig. 7 we present graphs similar to those of Fig. 6, except that in this figure the angle of incidence corresponding to a given number of decibels down from the σ^0 level at normal incidence is plotted vs the wind speed. Any one of these curves can serve as a measure of the wind velocity or of the roughness of the sea surface.

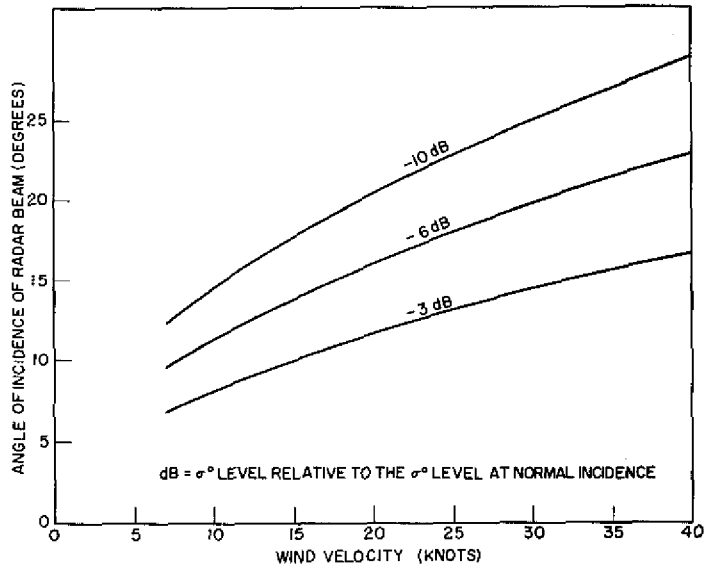

Fig. 7 - The angle of incidence at a given wind velocity necessary to maintain σ^0 at a constant level of N dB relative to σ^0 at normal incidence; N = -3, -6, and -10

At the steep angles of the wave paths through the troposphere used in this problem, the error introduced by refraction is negligible. At great radar heights above the sea, it becomes necessary to take into account the curvature of the earth in the determination of the angle of incidence of the radar beam at the sea surface corresponding to the angle of the beam off vertical at the radar site.

PART II—STUDY OF σ^0 NEAR NORMAL INCIDENCE USING SCHOOLEY FACET MODEL

Background

The data of Schooley (1) published in 1962 on the statistics of wind-disturbed water waves using the facet concept provide at least one experimental model upon which a study of σ^0 at near normal incidence can be undertaken. Without attempting to justify the facet model, suffice it to say that the upwind-downwind ratios reported by Schooley did tend to be substantiated to some extent by the available sea data. In this second part of this report the purpose is to use the Schooley statistics applied to the calculation of σ^0 vs radar wavelength and wind velocity at normal incidence and at angles from normal up to no greater than 40 degrees. The study will consider the same factors affecting σ^0 as did the theoretical analysis in Part I. The results show remarkable similarities despite the fact that the models are rather disparate.

Calculations of σ^0 at Normal Incidence

The Schooley data take the form of two distributions: (a) the probability density of facet inclination angles and (b) the distribution of average facet length vs facet inclination angle and wind velocity. In Fig. 8 a typical inclination-angle density curve is shown for a 10-knot wind. Similar curves also exist for 15- and 20-knot winds. In Fig. 9 a typical set of facet curves is shown for a radar wavelength of $\lambda = 3$ cm and 10-, 15-, and 20-knot winds. Curves also exist for $\lambda = 1$, 5, and 10 cm. It should be noted that the probability density curves are not Gaussian, although they do look somewhat bell shaped. These are one-dimensional cuts in the direction of the wind and are thus skewed. Also the tails are unsymmetrical. In computing σ^0 using the facet model, it is assumed

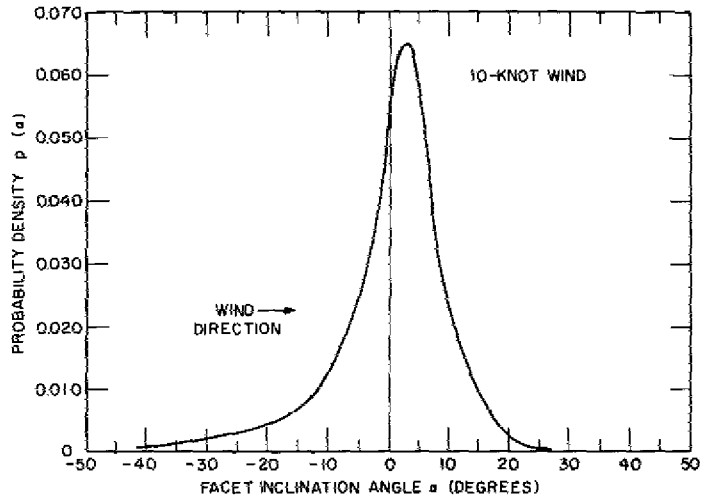

Fig. 8 – Probability density of facet inclination angles for a 10-knot wind

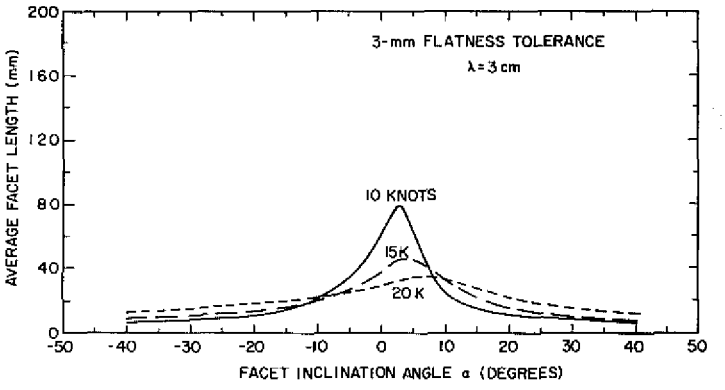

Fig. 9 - Distribution of average facet lengths at a radar wavelength of λ = 3 cm for wind velocities of 10, 15, and 20 knots

that the facets are flat circular disks of diameter given by the Schooley average facet length. The effective radar scattering area A_e is determined from the actual area A and the a/λ ratio, where a is the facet radius, by using the theoretical curve of Schmitt (10) also reproduced by Schooley (1). In computing σ^0, the total expected radar return from the scatterers σ is obtained by summing over the facet inclination-angle probability densities as follows:

$$\sigma = \sum_{\substack{\text{over}\\ \text{all}\\ \text{facets}}} p\,(\alpha_i)\,(A_e)i\,|R_S(0)|^2, \tag{21}$$

where $p\,(\alpha_i)$ is the probability density of the facet angles of inclination α_i and $|R_S(0)|^2$ as defined in Part I is taken to be 0.65. To calculate the effective area illuminated by the radar beam, we use

$$A_{iii} = \sum_{\substack{\text{over}\\ \text{all}\\ \text{facets}}} p\,(\alpha_i)\,A_i\,\cos\,\alpha_i\,, \tag{22}$$

which gives the projected area of the beam on the mean surface level of the sea. The value of σ^0 is then obtained from

$$\sigma^0 = \sigma/A_{iii}. \tag{23}$$

The results of these calculations are shown for normal incidence in Fig. 10. The limited data available permit only three values of wind velocity to be plotted. The curves show moderate variations of σ^0 with wavelength at the lower wind velocities; all show the expected decrease in σ^0 as the wind velocity increases. The curve obtained in Part I using the specular point model is superimposed for comparison. The similarity is striking. The agreement of σ^0 values is closer than expected for such diverse models.

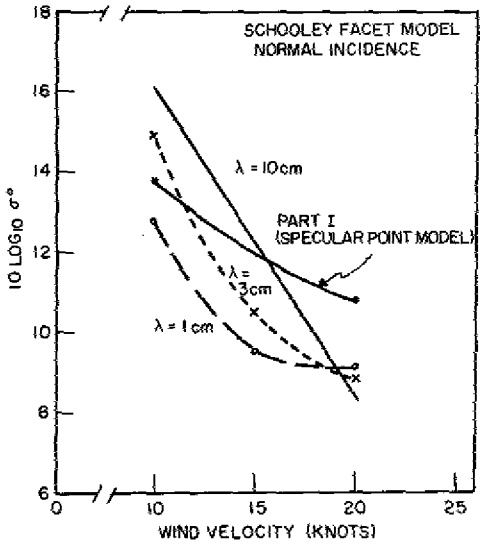

Fig. 10 - Clutter values of σ^0 at normal incidence vs wind velocity for radar wavelengths of λ = 1, 3, and 10 cm

Calculations of σ^0 Near Normal Incidence

In order to compare the facet model with the specular point model of Part I, calculations are made of σ^0 for angles of incidence off the normal. One requirement here is the determination of the radiation pattern from the facets to establish whether or not the scattered energy is seen by the radar. The half-power beamwidth of the main lobe from a flat circular disk is given by Silver (11) as

$$\psi = 2 \sin^{-1} \left(0.51 \frac{\lambda}{D}\right), \tag{24}$$

where $D = 2a$ is the diameter of the facet.

To simplify the calculations, it is assumed that if the radar beam lies within these half-power points, then all scattered energy from the facet is returned to the radar, whereas in cases where the radar beam is outside the half-power points none of the reradiation is seen by the radar. The geometry for a radar looking upwind is shown in Fig. 11, from which we have the condition for full backscatter,

$$\gamma < \left(\frac{\psi}{2} + \alpha\right). \tag{25}$$

The corresponding geometry for a radar looking downwind is shown in Fig. 12, from which the condition for full backscatter is

$$\gamma < \left(\frac{\psi}{2} - \alpha\right). \tag{26}$$

The results of calculations at λ = 3 cm only are presented in Fig. 13, showing the effect of wind velocity on σ^0 with respect to the radar angle of incidence. It is noted that, as in Part I, the maximum value of σ^0 is greater and the slope is steeper for the lower wind velocities. Further, these curves show a difference in clutter return between a radar looking upwind and one looking downwind. The reason for this is the unsymmetrical and skewed slope probability distribution in the measured data. Such a difference

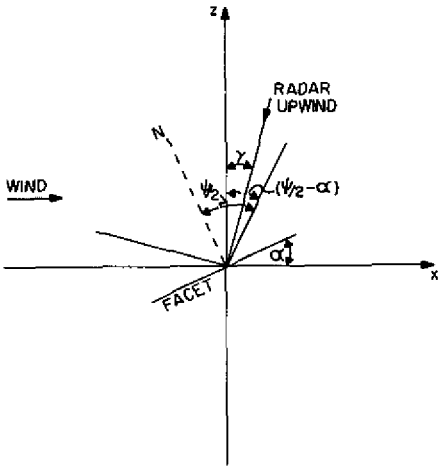

Fig. 11 - Geometry of radar-to-facet interface for a radar looking upwind

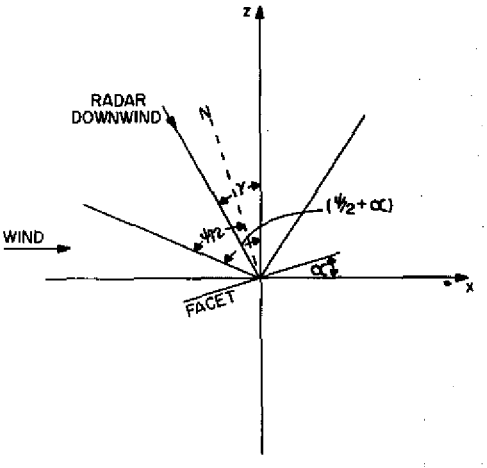

Fig. 12 - Geometry of radar-to-facet interface for a radar looking downwind

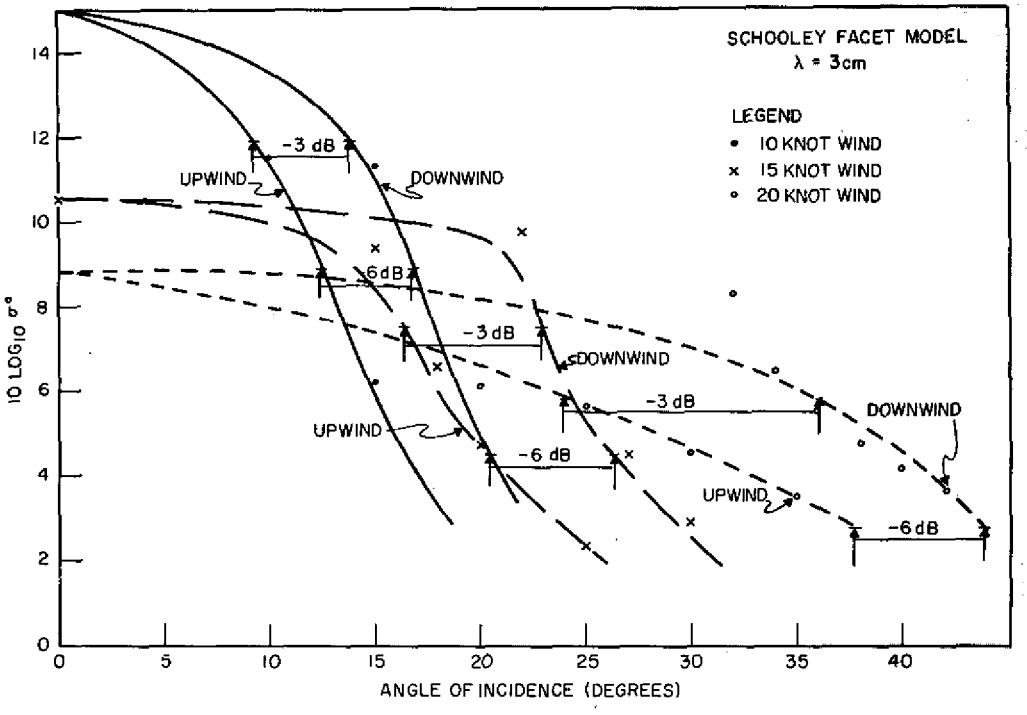

Fig. 13 - Upwind and downwind clutter σ^0 vs radar angle of incidence at λ = 3 cm for wind velocities of 10, 15, and 20 knots

was not present in the theory of Part I because of the Gaussian assumption for wave slope density. Also, it should be remembered that the analysis in Part I is two-dimensional and the Schooley data used in Part II are only one-dimensional.

In Fig. 11 the points where σ^0 is 3 and 6 dB down from maximum are indicated by arrows. Extracting these points in separate plots produces curves similar to Fig. 7 of Part I. Curves for the upwind σ^0 differences with angle of incidence vs wind velocity are in Fig. 14, and curves for the downwind differences are in Fig. 15. In order to plot these curves vs the mean square slope $\overline{S^2}$, calculations with the Schooley data were made using the formula

$$\overline{S^2} = \sum \tan^2 \alpha_j \, p(\alpha_j) - \left[\sum \tan \alpha_j \, p(\alpha_j)\right]^2. \tag{27}$$

A plot of this relationship, which is independent of frequency, is shown in Fig. 16. With this curve, the differences of Figs. 14 and 15 can be plotted vs $\overline{S^2}$ and are shown in Figs. 17 and 18. A comparison at the -3 dB level with Fig. 6 in Part I reveals the same type of straight-line curve with positive slope. However, the slope is far less in the specular point theoretical model than it is in the measured facet model.

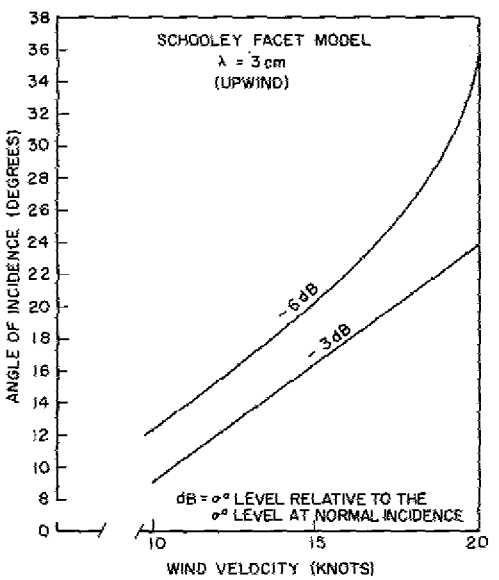

Fig. 14 - Upwind contours at the -3 and -6 dB levels showing radar angle of incidence vs wind velocity

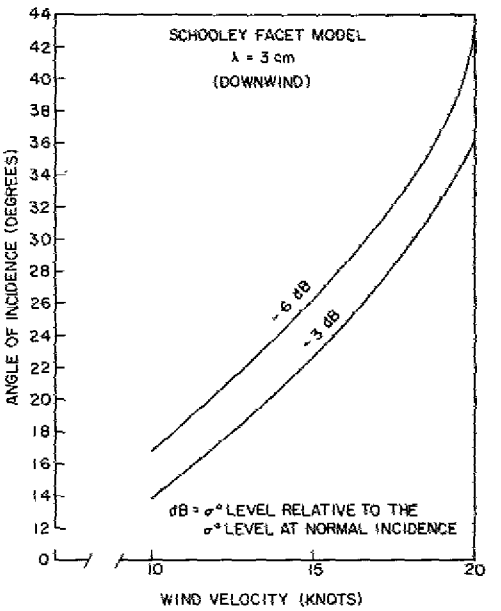

Fig. 15 - Downwind contours at the -3 and -6 dB levels showing radar angle of incidence vs wind velocity

A COMPARISON OF THE SPECULAR POINT AND SCHOOLEY FACET MODELS

The specular point model of Kodis takes into account the relative phases of the back-scattered fields from the many elementary areas of the illuminated surface of the sea in the derivation of the radar cross section of the sea. According to Kodis, because of the random nature of the surface and as a result of the roughness vs wavelength restriction, contributions from the interaction of pairs of specular points tend to cancel. In this

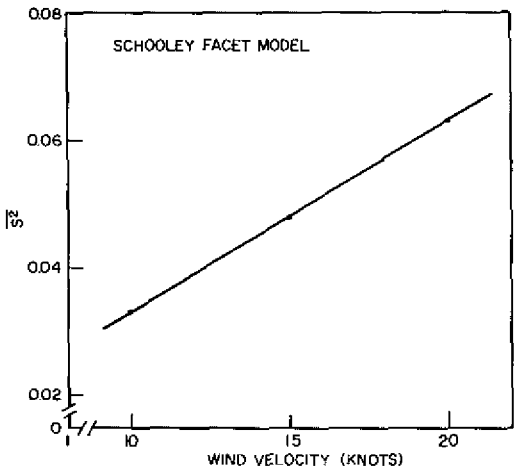

Fig. 16 – Plot of mean square facet slope $\overline{s^2}$ vs wind velocity using Schooley data

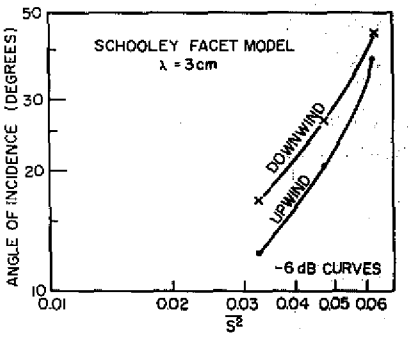

Fig. 17 – Upwind and downwind contours at the -3 dB level showing radar angle of incidence vs $\overline{s^2}$

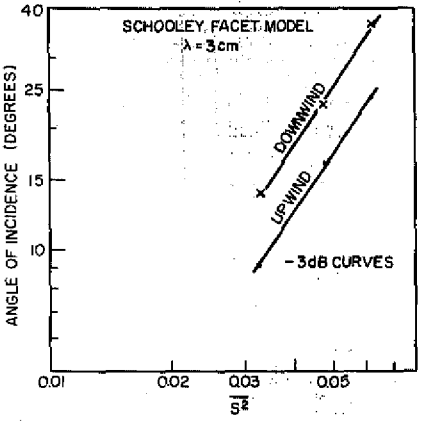

Fig. 18 – Upwind and downwind contours at the -6 dB level showing radar angle of incidence vs $\overline{s^2}$

model the sea is treated as a two-dimensional random surface with a Gaussian probability distribution of surface slope. The sea is considered isotropic, that is the wave motion has no preferred direction. The specular point model utilizes the usual physical optics approximations that make σ^0 independent of frequency and polarization. The shorter the radar wavelength, the more accurate the approximations become.

The Schooley facet model is a one-dimensional model wherein the radar cross section of the sea represents the sum of the cross sections of the individual facets of the surface independent of the phase relations between the backscattered field components of the facets. The angles of inclination of the facets possess a non-Gaussian probability distribution function such as the one shown in Fig. 8. The somewhat bell-shaped probability density curves represent one-dimensional cuts in the direction of the wind and thus exhibit skewness and asymmetry. In the facet model an attempt is made to account for the diffraction effects of the facets of the sea surface. The frequency dependence exhibited by the facet model comes about from the diffraction effects.

The Schooley facet model uses two sets of measured data: (a) the probability density of facet angles of inclination with wind speed as the parameter, and (b) the curves of average facet length vs facet angle of inclination. Since the second set of curves is obtained

by averaging, sometimes over a very limited sample, the results are subject to some inaccuracies. No doubt this is a factor entering into the somewhat different σ^0 characteristics exhibited by the two models considered in this report.

In the facet model, both large- and small-scale roughness of the sea surface are taken into account in arriving at σ^0. In the specular point model, only the large-scale roughness of the sea surface affects σ^0. Areas of the sea surface oriented normal to the line of sight are responsible for the backscattered power in the case of large-scale roughness; hence, this component dominates the radar cross section of the sea in the vicinity of normal incidence.

CONCLUSIONS

It is shown in Part I that the radar cross section per unit area of the sea is given approximately by the same formula as the one Barrick derived for a plane wave incident on the sea surface provided the inequalities appearing in Eqs. (15) and (16) hold for any combination of mean square slope of the sea surface, the antenna beam width, and the angle of incidence of the antenna beam.

The theoretical values of σ^0 of Part I have been compared with the experimental values determined by Grant and Yaplee. The agreement is found to be quite good at a wavelength of 8.6 mm (on the order of 1- to 1.8-dB difference) and at wind speeds of 14 to 25 knots, but the agreement is much poorer for a wind speed of 7 knots. This lack of agreement should not have been unexpected, since the theory is based on a "rough" surface and the basic assumptions on roughness appear to be violated as the wind speed diminishes. At longer wavelengths the experimental data departs by a greater margin from the theoretical. This may be partly because the relationship between $\overline{S^2}$ and wind speed used here was obtained from optical measurements.

The two sea return models described do not agree in quantitative detail, but there are striking similarities. To confirm the theory, further experimental measurements of the deviation of the angle of incidence of the radar beam off vertical necessary to reduce σ^0 in level by 3 dB would be required under various sea conditions. It is possible that this measure of radar sea return could be correlated with the character of the sea surface as found by optical sensors and processing. The optical information characterizing the surface of the sea could be correlated with the speed, fetch, and duration of the wind.

REFERENCES

1. Schooley, A.H., "Upwind-Downwind Ratio of Radar Return Calculated from Facet Size Statistics of a Wind-Disturbed Water Surface," Proc. IRE 50:456-461 (Apr. 1962)

2. Kodis, R.D., "A Note on the Theory of Scattering from an Irregular Surface," IEEE Trans. Antennas and Propagation AP-14:77-82 (Jan. 1966)

3. Isakovich, M., "The Scattering of Waves from a Statistically Rough Surface," Zhur. i Eksp. Teoret. Fiz. 23:305-314 (1952), English translation by M. Friedman

4. Hagfors, T., "Backscattering from an Undulating Surface with Applications to Radar Returns from the Moon," J. Geophys. Research 69:3779-3784 (1964)

5. Semenov, B.I., "Scattering of Electromagnetic Waves by Bounded Regions of Rough Surfaces Having Finite Conductivity," Radiotekh. i Elektron. 10:1952-1960 (1965); Radio Engrg. Electron. Phys. 10:1666-1673 (1965)

6. Stogryn, A., "Electromagnetic Scattering from Rough, Finitely Conducting Surfaces," Radio Sci. 2:415-428 (1967)

7. Barrick, D.E., "Rough Surface Scattering Based on the Specular Point Theory," IEEE Trans. Antennas and Propagation AP-16:449-454 (July 1968)

8. Cox, C., and Munk, W., "Measurement of the Roughness of the Sea Surface from Photographs of the Sun's Glitter," J. Opt. Soc. Am. 44:838-850 (Nov. 1954)

9. Grant, C.R., and Yaplee, B.S., "Back Scattering from Water and Land at Centimeter and Millimeter Wavelengths," Proc. IRE 45:976-982 (July 1957)

10. Schmitt, H.J., "Back-Scattering Measurements with Space-Separation Method," Cruft Lab., Harvard Univ., Cambridge, Mass., Scientific Rept. No. 14, Nov. 1957

11. Silver, S., editor, "Microwave Antenna Theory and Design," M.I.T. Rad. Lab. Ser., New York:McGraw-Hill, 12, p. 194, Eq. (74), 1949

Appendix

A MORE GENERAL EXPRESSION FOR σ^0 AT NORMAL INCIDENCE

It turns out that an expression for the radar cross section per unit area of the sea for normal incidence can be derived without the restrictions on the calmness of the sea and the beamwidth of the radiation pattern of the radar antenna. Such restrictions were used to develop the formula for σ^0 for other than normal incidence, Eq. (14).

Beginning with Eq. (5) with a set equal to zero, we evaluate the integral by integrating twice by parts to obtain the following expression for the radar cross section of a circular illuminated area of the sea:

$$\sigma_S = \pi h_0^2 \, |R_S(0)|^2 \left[\left(1 + 2\overline{S^2} + 2\left(\overline{S^2}\right)^2\right) - \left(\sec^4 \theta_0 + 2\overline{S^2} \sec^2 \theta_0 + 2\left(\overline{S^2}\right)^2\right)\right.$$

$$\left. \exp\left(-\tan^2 \theta_0\right)/\overline{S^2}\right], \tag{A1}$$

where the radius of the illuminated area is $h_0 \tan \theta_0$. The illuminated area of the sea is $\pi h_0^2 \tan^2 \theta_0 / \langle |\cos \beta| \rangle$; hence, σ^0 for normal incidence is given by the expression

$$\sigma^0 = \frac{\sigma_S}{\pi h_0^2 \tan^2 \theta_0 / \langle |\cos \beta| \rangle}$$

$$\sigma^0 = \frac{|R_s(0)|^2 \langle |\cos \beta| \rangle}{\tan^2 \theta_0} \left[\left(1 + 2\overline{S^2} + 2\left(\overline{S^2}\right)^2\right) - \left(\sec^4 \theta_0 + 2\overline{S^2} \sec^2 \theta_0 + 2\left(\overline{S^2}\right)^2\right)\right.$$

$$\left. \exp\left(-\tan^2 \theta_0 / \overline{S^2}\right)\right]. \tag{A2}$$